Available online at:
ogst.ifpenergiesnouvelles.fr

REGULAR ARTICLE

OPEN ⌬ ACCESS

Enhancing surfactant desorption through low salinity water post-flush during Enhanced Oil Recovery

Ichhuy Ngo[1,2,*] ⓘ, Kyuro Sasaki[2], Liqiang Ma[1,*] ⓘ, Ronald Nguele[2] ⓘ, and Yuichi Sugai[2]

[1] Key Laboratory of Deep Coal Resource Mining, China University of Mining & Technology, Ministry of Education, Xuzhou 221116, China
[2] Resources Production and Safety Engineering Laboratory, Department of Earth Resources Engineering, Kyushu University, Fukuoka 819-0395, Japan

Abstract. Low Salinity Water (LSW) incorporates in surfactant Enhanced Oil Recovery (EOR) as a pre-flush is a common practice aiming to reduce the formation salinity, which affects surfactant adsorption. However, in a field implementation, the adsorption of surfactant is unavoidable, so creating a scheme that detaches the trapped surfactant is equally essential. In this study, LSW was a candidate to enhance the desorption of surfactant. LSW solely formulated from NaCl (1 wt.%), Sodium Dodecylbenzene Sulfonate (SDBS) was chosen as the primary surfactant at its critical micelle concentration (CMC, 0.1 wt.%). It found that injecting LSW as post-flush achieved up to 71.7% of SDBS desorption that lower interfacial tension against oil (31.06° API) to 1.3 mN/m hence bring the total Recovery Factor (RF) to 56.1%. It was 4.9% higher than when LSW injecting as pre-flush and 5.2% greater than conventional surfactant flooding (without LSW). Chemical analysis unveiled salinity reduction induces Na^+ ion adsorption substitution onto pore surface resulting in an increment in surfactant desorption. The study was further conducted in a numerical simulation upon history matched with core-flood data reported previously. By introducing LSW in post-flush after SDBS injection, up to 5.6% RF increased in comparison to other schemes. The proposed scheme resolved the problems of adsorbed surfactant after EOR, and further improve the economic viability of surfactant EOR.

1 Introduction

After primary and secondary recoveries, subsequent volumes of oil are still trapped within the porous media. At this stage, inner or external driving forces are not adequate to push the stranded oil due to the narrow pore throat, oil-wet pore surfaces, High Interfacial Tension (IFT) between oil and aqueous phases, and unfavorable capillary conditions [1–5]. Enhanced Oil Recovery (EOR) techniques have been developed to increase oil production using different approaches based on various reservoir conditions. One of which is the Chemical EOR (CEOR), where chemical solutions; for instance, alkali, surfactant, polymer, or injecting them as sequences into the oil-bearing reservoir.

Extensive researches have been conducted to unveil the underlying recovery mechanisms of surfactant flooding. Yuan *et al.* and Jang *et al.* addressed that adding surfactant leads to decrease capillary forces and IFT of the fluids [6, 7]. Added surfactant first lowers IFT between oil and water phases, which thereby produce *in-situ* emulsions and/or microemulsion [8, 9]. In the form of an emulsion, the size

of released oil droplets is minimized. In this regard, the flow restriction due to the narrow pore-throat is mitigated, the capillary force decreases, hence increase oil recovery. Mandal *et al.* studied the role of oil-in-water emulsion in EOR found an increase of 20% Original Oil In Place (OOIP) over conventional waterflooding [10]. Later Zhao *et al.* compared the effect of Sodium Oleate (SOL) and Sodium Dodecylbenzene Sulfonate (SDBS) [11]. They found that the former recovered 17% of oil comparing to 8% by the latter, it was due to the ultra-low IFT and emulsification, respectively.

Along with the wealth of surfactant injection, other researchers [12, 13] equally reported the weaknesses of the surfactant EOR. Apart from salting-out effects and temperature tolerance, surfactant adsorption onto pore surfaces greatly reduces its economic attractiveness. The degree of adsorption is affected by salinity, formation brine hardness, temperature, and surfactant polar and rock surface charge [14, 15]. Ngo *et al.* reported up to 57.7 mg/100 g-rock of SDBS adsorption on Berea sandstone surface [16]. Ngo *et al.* later added that by increasing salinity from 1 to 3 and 5 wt.% NaCl, the adsorption was doubled that reduced up to 4.6% of oil recovery [17].

* Corresponding authors: tbh230@cumt.edu.cn; ckma@cumt.edu.cn

In this regard, Low Salinity Water Flooding (LSWF) has been developed to enhance oil recovery on its own [18, 19] and to corporate with gas [20] or other active chemicals such as a surfactant [21]. Sheng reviewed that approximately 17 mechanisms pertaining to solely LSWF, among which fine migration, mineral dissolution, Multicomponent Ion Exchange (MIE), and wettability alteration stood as prominent [22]. Extensive works [23–26] presented comprehensive results regarding the effects of ion types on the effectiveness of LSWF. They found that SO_4^{2-} is the most dominant in driving rock to less oil wetness. As for combined injection, the corporate LSW reduces the salinity of the formation before surfactant injection aims at reducing surfactant adsorption. Moreover, Hosseinzade Khanamiri *et al.* reported that LSWF and Low Salinity Surfactant (LSS) both have the potential to shift the wettability of the rock to more water-wet conditions comparatively to High Salinity Water (HSW) and High Salinity Surfactant (HSS) [27]. Tavassoli *et al.* further elucidated that the injection of LSW prior surfactant solution recovered up to 94.4% of RF comparing to 74.5% by HSW [28]. Araz and Kamyabi [29] later debated that wettability shifted from water to neutral wet is as well favorable to enhanced RF, where up to 9.2% OOIP was additionally produced by injecting LSS after LSW.

From the efforts of literature, most researches focused on the prevention of surfactant adsorption, which is a great practice to increase the economic viability of surfactant flooding. However, we could see that the surfactant adsorption still takes place regardless of the degree of adherent. To the best of our knowledge, a few pieces of research have depicted the surfactant adsorption is reversible [17, 30, 31]. The effect of surfactant desorption on oil recovery and its underlying mechanisms has less regard, so the approaches to increase surfactant desorption were as well less popular. This study, therefore, aims to fill in this gap by evaluating the importance of surfactant desorption and proposing an injection scheme to enhance desorption. Using SDBS as the primary surfactant solution, it was injected right after the Formation Brine (FB). In this study, surfactant was allowed to adsorb onto pore surfaces without any pre-treatment. The LSW was injected in post-flush to enhance surfactant desorption. The effectiveness of (1) the proposed work (LSW-SDBS-FB) was evaluated with (2) conventional surfactant flooding (HSW-SDBS-FB) and (3) combined LSW-surfactant flooding (LSW-SDBS-LSW). We further investigated the underlying mechanisms through chemical analysis of the producing effluent. After which, the proposed injection sequence was implemented in a reservoir simulator, STARS, to validate its applicability on a field scale.

2 Experimental sections

2.1 Surfactant solution, synthetic water, oil sample, and reservoir rock

Sodium Dodecylbenzene Sulfonate (SDBS), an anionic surfactant, 99.99% pure supplied by *Sigma Aldrich* (Japan) chosen in this study due to its availability in petroleum in

industry. The aqueous solution of SDBS was preparing at its critical micelle concentration (CMC, 0.1 wt.%), determined following Interfacial Tension (IFT) reduction approach, using DropMaster (model DMS-401).

A total salinity of 3 wt.% of synthetic Formation Brine (FB), representative of that of the candidate oil field, was formulated in-house from sodium chloride (NaCl), calcium chloride ($CaCl_2$), magnesium chloride ($MgCl_2$), potassium chloride (KCl), sodium sulfate (Na_2SO_4) and sodium bicarbonate ($NaHCO_3$). High Salinity Water (HSW) and Low Salinity Water (LSW) at 3 and 1 wt.% were preparing from sodium chloride (NaCl, 99.99% pure). The chemicals were purchased from *Junsei Chemical* (Japan). The chemical compositions of FB, HSW, and LSW were outlined in Table 1.

The candidate oil is the dead light oil sampled from a Japanese oil field where the bottom-hole temperature is 45 °C. The oil has an API of 31.06°, a density of 867.6 kg/m³, an absolute viscosity of 5.67 mPa.s at 45 °C, and a Total Acid Number (TAN) of 1.86 mg KOH/g oil.

Berea sandstone, representative of the targeted oil-bearing matrix, was selected for the core-flood test. The porosity and permeability were determined prior to core-flooding experiments by water saturation and water flowing tests, respectively. The mineral compositions of sandstone were investigated by X-Ray Diffraction spectroscopy (XRD, *Bruker D8 Advance*, Germany). Figure 1 presents the SEM image and XRD spectra of the candidate sandstone. The main mineral compositions are quartz (SiO_2) along with a small proportion of albite ($NaAlSi_3O_8$) and kaolinite ($Al_2Si_2O_5(OH)_4$).

2.2 Core-flooding

Core-flood was conducted in an apparatus schematized in Figure 2.

The injection was performing at the reservoir temperature of 45 °C. Before core-flooding tests, we determined both the porosity and Pore Volume (PV) of the core (7.23 cm in length, 4.53 cm in diameter) by the fluid saturation method. The core was then dried in the oven for 12 h at a constant temperature of 110 °C to remove residual water content within, following which the weight of the dried core was recorded. Permeability of the core was determined by the freshwater flowing test. Three PV of freshwater was injecting at a constant flow rate of 0.5, 1, and 1.5 mL/min. The absolute permeability was then obtained from Darcy's law (Eq. (1)):

$$Q = \frac{K_{abs}}{\mu} \times \frac{A\Delta P}{L}, \tag{1}$$

where Q is the flow rate (m³/s), K_{abs} is the absolute permeability (m²), u is the water viscosity (in Ns/m²), A is a cross-section of the core (m²), ΔP is the pressure drop across the core (Pa), L is the length of the core (m).

Once mounted in the Hassler core holder, FB was initially imbibed into the core to displace the *in-situ* fresh water. The injection was conducted for 3 PV to ensure the salinity of the core reach formation condition. Then, an oil sample was injecting to drain FB until initial

Table 1. Synthetic brine and low salinity water composition (wt.%).

Ionic composition	Na^+	Ca^{2+}	Mg^{2+}	K^+	Cl^-	SO_4^{2-}	HCO_3^-	TDS	pH
FB	0.94	0.09	0.03	0.03	1.61	0.28	0.01	3.00	5.1
LSW	0.39	–	–	–	0.61	–	–	1.00	5.3
HSW	1.18	–	–	–	1.82	–	–	3.00	5.1
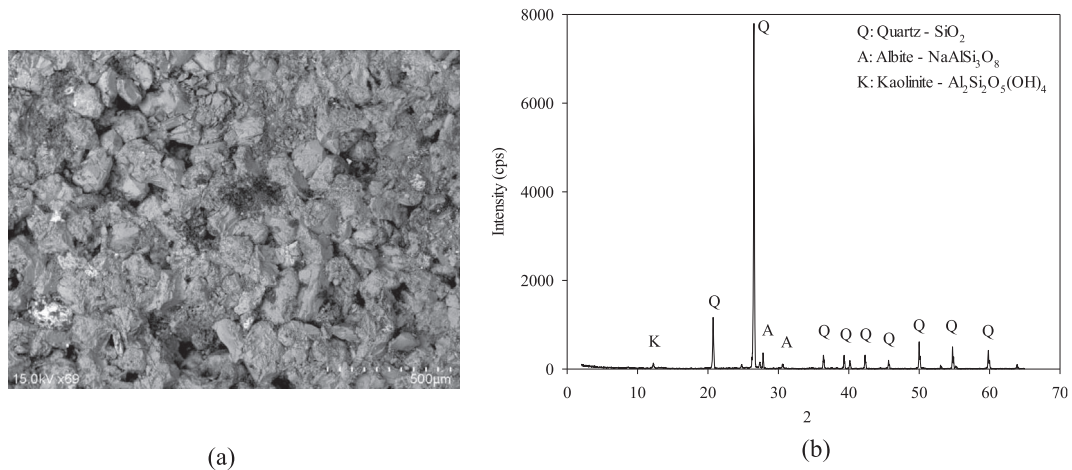
Fig. 1. SEM and XRD of the Berea sandstone. (a) SEM image. (b) XRD spectra.
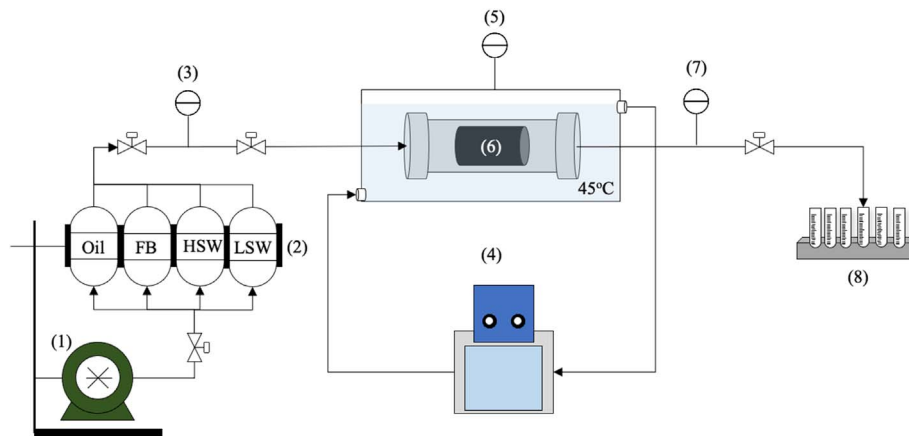
Fig. 2. Schematic representation of core-flooding apparatus; (1) pump, (2) jacketed cell containing injecting fluids (oil, FB, HSW, and LSW), (3) injector pressure indicator, (4) thermostatic bath, (5) temperature indicator, (6) Hassler core holder, (7) back pressure regulator, (8) fractionator.

water saturation (S_{wi}). The injection was controlling at 1 mL/min. As a base of comparison, the following injection scenarios were conducted:

1. HSW → SDBS → FB: FB was injecting at 1 mL/min in the pre-flush until no more or less than 1% in the fractionator. SDBS solution was injecting for 1 PV at 0.5 mL/min. HSW was used to drive free oil and SDBS to the production end, performing at 1 mL/min for 6 PV. This scheme is a base case in conventional surfactant flooding, aiming at serving as a comparison to other approaches.

2. LSW → SDBS → LSW: In maintaining injecting PV and flow rate, SDBS slug was injecting in between two LSW slug in pre-flush and post-flush. This scenario represents the current combined EOR of surfactant and LSW. The technique prevents the adsorption of surfactant to the formation when enhancing oil production.

3. LSW → SDBS → FB: This scheme differs from LSW-SDBS-LSW by which FB was injecting in pre-flush. The pre-treatment on SDBS adsorption was neglected. The study aims at resolving the situation where surfactant has already adsorbed within the
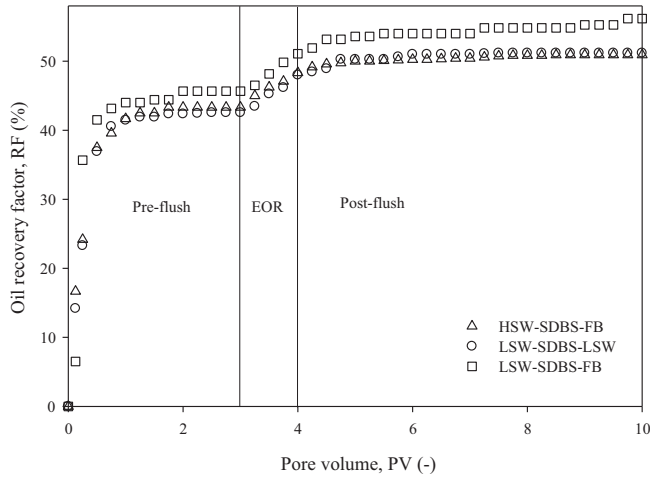
Fig. 3. Oil Recovery Factor (RF) against injecting PV of HSW-SDBS-FB, LSW-SDBS-LSW, and LSW-SDBS-FB.

formation. We proposed to inject LSW at the trail of the SDBS slug to investigate the effects such as surfactant desorption, oil Recovery Factor (RF), and other underlying mechanisms.

2.3 Chemistry of the effluent

The effluent of core-flood was collected throughout the experiment to determine the concentration of SDBS and sodium ion (Na^+). The concentration of SDBS was determined following the Beer-Lambert principle using a UV-visible spectrophotometer (model 2450, *Shimadzu*), where Na^+ was measured by Laqua Twin Meter (model S022, *Horiba Scientific*, Japan).

3 Results and discussion

3.1 Oil recovery

We evaluated the common combined LSW-surfactant (LSW-SDBS-LSW) and our proposed scheme surfactant-LSW (LSW-SDBS-FB), where conventional surfactant flooding (HSW-SDBS-FB) equally performed as a base of comparison. The results showed in Figure 3.

It is worth highlighting that injection of LSW in pre-flush gave an insignificant effect; for instance, the RF was 42.5% that is 3.2% lower than which of FB injection. It is plausibly affected by the initial oil saturation. The core used in LSW-SDBS-LSW's scenario was 75.2%, which is 5.2% lower than LSW-SDBS-FB as summarized in Table 2. However, the effect of pre-LSW injection was observed after SDBS injection. The pre-injection of LSW led to the highest RF of 5.5%, which was 0.5% higher than HSW-SDBS-FB conventional surfactant flooding. The benefit continued to post-flush, where RF of LSW-SDBS-LSW was 3.2% which is 0.6% higher than which of HSW-SDBS-FB.

In the LSW-SDBS-FB scheme, the injection LSW in post-flush revealed a significant enhancement over other cases, where RF was 5.1% that is 1.9% greater than which of LSW-SDBS-LSW. The higher recovery over HSW-SDBS-FB is easy to understand due to the higher adsorption of surfactant onto pore surfaces in a higher salinity environment [32]. However, injecting the same LSW in LSW-SDBS-FB and LSW-SDBS-LSW cases must be associated with other underlying mechanisms that drive different effectiveness. Therefore, we measured sodium (Na), SDBS concentration, and IFT of the effluent solution.

3.2 Chemistry of effluent and IFT

To understand the mechanism of our proposed scheme, we tracked Na ion, SDBS concentration in the effluent of the core-flooding experiments. The results showed in Figure 4.

Looking at the evolution of Na of LSW-SDBS-LSW, a monotonic decrease during pre-flush followed by a continued increase after SDBS injection. The continued increase of Na was plausibly from SDBS ($CH_3(CH_2)_{11}C_6H_4SO_3Na$) desorption and Na dissolution from NaCl salt and albite ($NaAlSi_3O_8$). The SDBS concentration monitoring in Figure 4b confirmed the desorption of SDBS during post-flush, but the desorption ends at 6 PV that accounted for 49.4% of recovered SDBS. It infers that the continued increase after 6 PV of Na was as well corresponds to Na dissolution. Based on the mineral compositions of the Berea sandstone core (Fig. 1), the increase of Na is plausibly due to weathering following the reaction path shown in equation (2) [33]:

$$\underset{\text{(albite)}}{NaAlSi_3O_8} + 8H_2O \underset{2}{\overset{1}{\rightleftharpoons}} Na^+ + Al(OH)_4^- + 3\big(4H^+; SiO_4^{4-}\big).$$

(2)
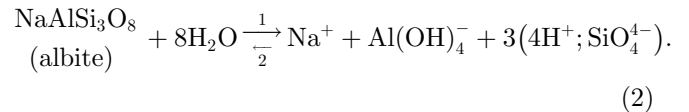
In the case of LSW-SDBS-FB, after a spike of Na during SDBS injection, it was further alleviated by the LSW (Fig. 4a). It leads to the thought that Na and SDBS fail to release from the pore surface. SDBS concentration in Figure 4b revealed a contrasting behavior against the hypothesis, where SDBS spiked at 4.6 PV and gradually decreased to 0 at 7.6 PV. From a material balance calculation, 71.7% of SDBS was recovered in the effluent. After the main slug, LSW in the post-flush develops other slugs of desorbed SDBS in the injecting phase. The desorbed SDBS thereby was carried through porous media to the production end. In this regard, the loss of Na must relate to the pore surface. Na ion tends to adsorb to the pore surface as a substitute to the SDBS monomer. As addressed by literature [34, 35] where Na of LSW induces multi-component ion exchange. The exchange follows a bi-procedure illustrated in Figure 5. LSW first lowers the compression force of the adsorbates on the pore surface through a salinity reduction. Then, the adsorption infinity of the SDBS monomer is not as significant, so Na in the post-flush can displace and substitute the adsorbed surfactant monomer (Fig. 5a). The desorption of SDBS thereby increases its concentration in the displacing phase.
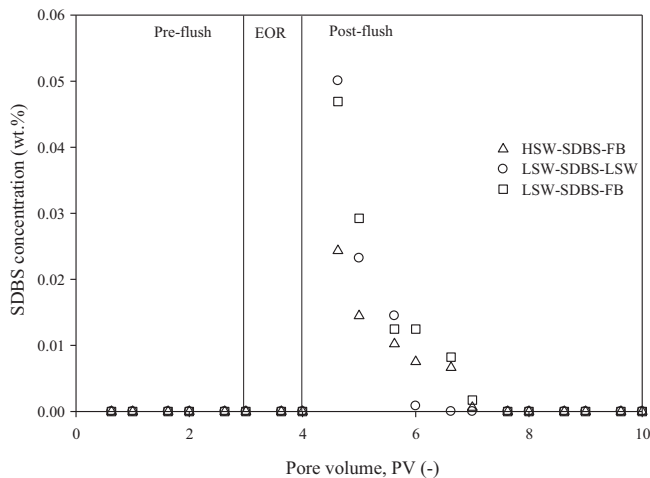
On contrary, due to the LSW pre-flush in LSW-SDBS-LSW, the SDBS adsorption was less prominent, hence

Table 2. Oil recovery summary.

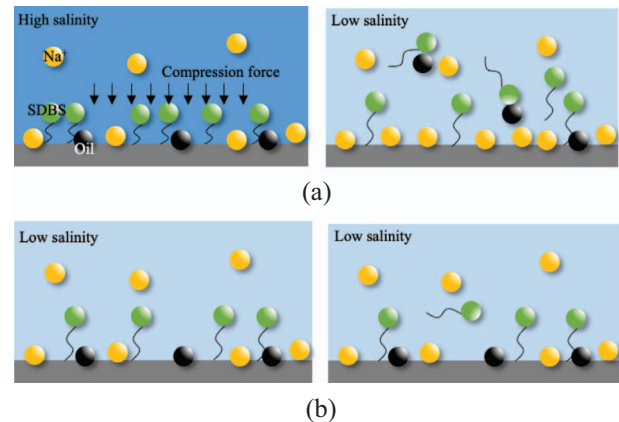| Scheme	Initial stage	Pre-flush	SDBS flooding	Post-flush
	Oil saturation (%)	RF (%)	RF (%)	RF (%)
HSW-SDBS-FB	77.9	43.3	5.0	2.6
LSW-SDBS-FB	80.4	45.7	5.4	5.1
LSW-SDBS-LSW	75.2	42.5	5.5	3.2
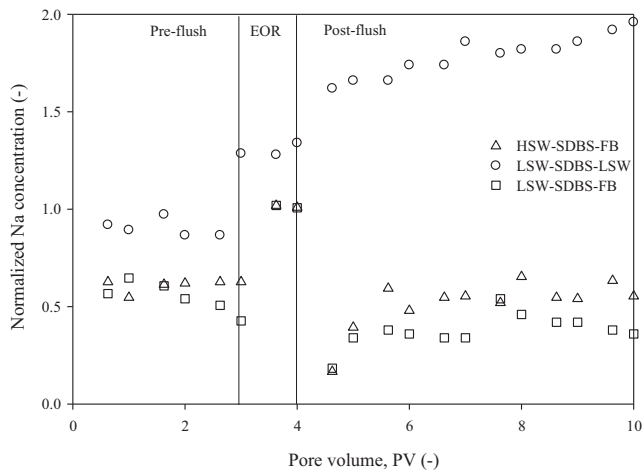
(a)

(b)

Fig. 4. Na and SDBS concentration during core-flooding experiments. (a) Normalized Na concentration. (b) SDBS concentration

Fig. 5. Illustration of Na and SDBS monomer behaviors during experiments. (a) LSW-SDBS-FB. (b) LSW-SDBS-LSW.

The collected effluent solution was utilized to measure IFT against the oil sample. The results are given in Table 3.

It observed that the IFT of LSW-SDBS-FB and LSW-SDBS-LSW was at 1.3 and 8.9 mN/m, respectively. The results agreed with the RF and chemistry of the effluent monitoring during core-flooding experiments. It aligns with our hypothesis; the proposed scheme is more effective than the current practice due to the greater desorption of SDBS. SDBS desorption was enhancing through the substitute adsorption of Na in the LSW. This is well agreed with Chai et al. [37], who addressed that the ionic composition has a great influence on crude oil-aqueous solution interaction, so the reduction of Na in the aqueous phase further improves the effectiveness of desorbed SDBS on the crude oil-aqueous interface. The Na desorption in LSW-SDBS-LSW however affects the effectiveness of SDBS in the post-flush.

From the above discussion, one could conclude that injection of LSW as the post-flush after SDBS enhanced RF owing to the mechanism of MIE. LSW first decreases the compression force applying on adsorbed SDBS monomers; Na ions in the LSW then replace the monomers. The increase in free monomers in crude oil-aqueous interface leads to a reduction in IFT, hence improve oil recovery.

To this point, there is a limitation in core-flooding experiments includes the number of schemes, injection slug size, and the performance of the work in a three-dimensional flow. To access the mentioned uncertainties, we performed a reservoir simulation using CMG-STAR 2019.10.

lower SDBS concentration in post-flush (Fig. 5b). LSW however unlocked Na from pore surface that will directly affect the interfacial activities of the desorbed SDBS. If this hypothesis is true, the IFT of effluent against oil should be lower in LSW-SDBS-FB than which of LSW-SDBS-LSW because of the electrolyte effect as addressed by Tichelkamp et al. [36].

Table 3. IFT of the effluent solution against oil sample.

Schemes	LSW-SDBS-LSW	LSW-SDBS-FB	HSW-SDBS-FB
Interface oil/effluent			
	8.9 mN/m	1.3 mN/m	9.5 mN/m

Table 4. Grid, fluid properties, and reservoir conditions.

Grid properties					Fluid properties				Reservoir conditions			
Dimension [block]	D [cm]	L [cm]	φ [%]	K [mD]	SDBS [wt.%]	FB [wt.%]	LSW [wt.%]	Oil [°API]	T [°C]	P_i [MPa]	S_{oi} [%]	S_{or} [%]
10 1 1	4.53	7.22	12.6	7.13	0.1	3	1	30.6	45	1	80.4	20

Table 5. Langmuir parameters (Ngo *et al.* [38])[a].

Isotherm	Correlation	R^2	q_{max}		K_{ad}, K_F
			Isotherm	Exp.	
Ads.	$1/q_e = 111.63/C_e + 0.56$	0.9986	1.786	1.723	0.016
Des. 3-1	$1/q_e = 82.23/C_e + 0.87$	0.9870	1.151	1.115	0.014
Des. 3-3	$1/q_e = 103.72/C_e + 0.61$	0.9858	1.643	1.569	0.016

[a] Ads.: Adsorption isotherm; Des. 3-1: Desorption isotherm with low salinity water; Des. 3-3: Desorption isotherm with high salinity water.

4 Reservoir model

4.1 Dynamic history matching of core-flooding experiment

History matching was conducting on a one-dimensional model of 10 blocks, which simulated fluids flow during core-flooding experiments. Fluids and reservoir properties of the model showed in Table 4. The injected fluid was simulating to flow in only one direction from injection to production wells that pre-set at first and tenth blocks, respectively. The conservation equation of flow follows equation (3). The adsorption and desorption of surfactant follow equations (4) and (5), where reversibility of surfactant was in a function of salinity within the formation. The effect of salinity on desorption was modeling followed by Ngo et al. [38]. The coefficients are revealed in Table 5. IFT between aqueous and oil phases is a function of SDBS concentration shown in equation (6) and in Table 6:

$$V\frac{\partial}{\partial t}\left[\varphi_f(\rho_w S_w w_i) + \varphi_v \mathrm{Ad}_i\right] = \sum_{k=1}^{n_f}\left[T_w \rho_w w_i \Delta\Phi_w\right]$$
$$+ V\sum_{k=1}^{n_f}(s'_{ki} - s_{ki})r'_k + \sum_{k=1}^{n_f}\left[\varphi D_{wi}\rho_w\Delta w_i\right]$$
$$+ \delta_{iw}\sum_{k=1}^{n_f}\rho_w q a q_{wk} + \rho_w q_{wk} w_i, \qquad (3)$$

where Δw_i is the water concentration differences between nodes (ppm), $\Delta\Phi_w$ is a potential difference of water (–),

Table 6. IFT, adsorption and desorption against SDBS concentration.

Concentration	IFT	Adsorption	Desorption
0	23.4	0	0
0.05	1.30	4.2	2
0.1	0.17	6	4.02

δ_{iw} is the distance between aquifers (cm), ρ_w is the density of water phase (g/cm^3), φ is the porosity (fraction), φ_f is the fluid porosity (fraction) and φ_v is the void porosity (fraction):

$$\mathrm{Ad} = \frac{(\mathrm{Tad1} + \mathrm{Tad2} \times x\mathrm{NaCl}) \times \mathrm{ca}}{(1 + \mathrm{Tad3} \times \mathrm{ca})}, \qquad (4)$$

$$C_f = C_i - \mathrm{Ad}, \qquad (5)$$

$$\mathrm{IFT} = F(C_f, x\mathrm{NaCl}), \qquad (6)$$

where Ad is the maximum adsorption (gmol/cm^3), Tad is the Langmuir parameters (gmol/cm^3), xNaCl is the salinity of the formation water (ppm), ca is the mole fraction, C_f is SDBS concentration after adsorption (wt.%), C_i is initial SDBS concentration (wt.%), IFT is the interfacial tension (mN/m).

Relative permeability to oil and water against water saturation, cumulative oil, and water production stands as the
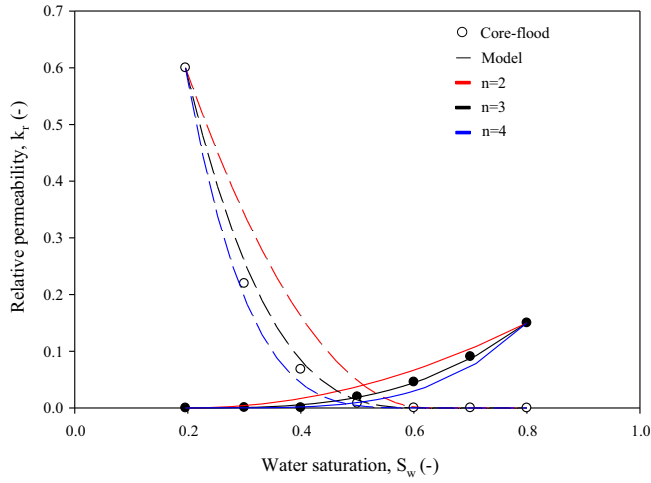
Fig. 6. Relative permeability to oil and water as a function of Corey exponent (n).

(a)

(b)

Fig. 7. Cumulative oil and water production fitting by capillary numbers. (a) Cumulative oil production. (b) Cumulative water production.

main parameters to validate the history matching. The flowability is the most critical parameter to simulate the oil and water flow within the core during the core-flooding experiment. However, the data of core internal properties such as pore size distribution, grain shape, and pore channel tortuosity are unavailable during core-flooding. The ease and difficulty of fluid passing between pores and pore-throats in porous media are described by power-law as written in equations (7) and (8). Corey exponent (n) is the parameter to control the flow behavior. Three sets of Corey exponent were presenting in this paper, where their matching degree gave in Figure 6:

$$k_{\mathrm{ro}} = k_{\mathrm{ro,max}} \left(\frac{S_{\mathrm{o}} - S_{\mathrm{or}}}{1 - S_{\mathrm{or}} - S_{\mathrm{wc}}} \right)^{n_{\mathrm{o}}}, \qquad (7)$$

$$k_{\mathrm{rw}} = k_{\mathrm{rw,max}} \left(\frac{S_{\mathrm{w}} - S_{\mathrm{wc}}}{1 - S_{\mathrm{or}} - S_{\mathrm{wc}}} \right)^{n_{\mathrm{w}}}, \qquad (8)$$

where k_{ro} and k_{rw} are relative permeability for oil and water [–], $k_{\mathrm{ro,max}}$ and $k_{\mathrm{rw,max}}$ are maximum relative permeability for oil and water [–], S_{o} and S_{w} are oil and water saturation [–], S_{or} is residual oil saturation [–], S_{wc} is critical water saturation [–], n_{o} and n_{w} are oil and water exponent [–].

The higher number of Corey exponent indicates a poor sorting of grain particles and the inclusion of clay and calcite particles, whereas the medium-range presents a better sorting, and the lower range indicates fractured formations. Investigating the plausible fractures developed by LSW injection is necessary [39]. As observed in the experimental section, MIE was the controlling mechanism, so fine migration could happen as addressed by Austad *et al.* [40]. To clarify, an exponent value of 2 was utilized to indicate fractured formation. As a hypothesis, if the core sample was fractured, the experimental results should be well fitted with an exponent value of 2. Herein, we showed the three
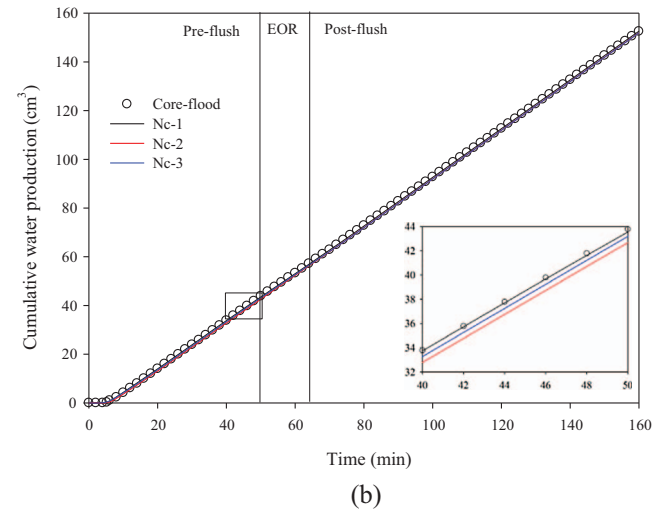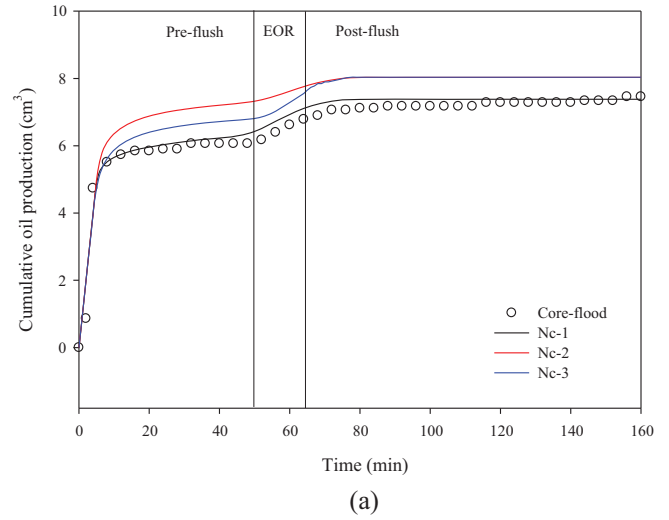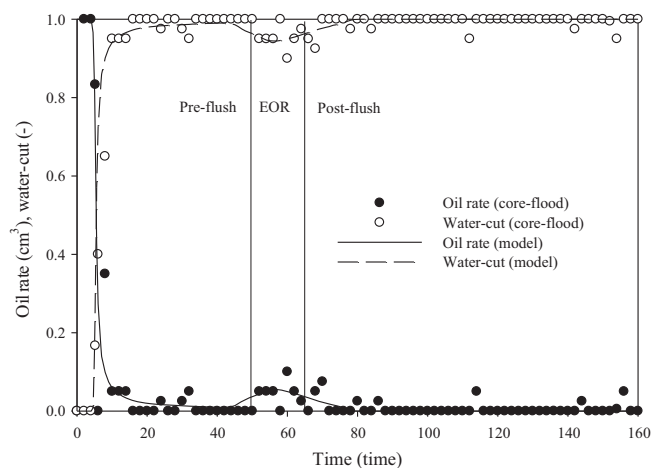
closest cases that include 2, 3, and 4 of the exponents. The exponent of 3 gave the best fitting curve comparing to 2 and 4 (Fig. 6). This inferred that there were no fractures developed during LSW injection. Thereby, Corey's exponent of 3 was utilized for further investigation.

Moreover, the capillary number is another controlling parameter in CEOR. As addressed by Sheng, increasing capillary number leads to higher recovery of residual oil [41]. He added that, in theory, an oil-bearing matrix is depleted once the capillary number is increased to 10^{-2} or 10^{-1}. In this regard, a set of capillary numbers was studied where the degree fitting error was evaluated by the cumulative oil and water production. Figure 7 illustrated the results of cumulative oil and water production by a variety of capillary numbers, and their summary gave in Table 7.

The capillary number randomly varied in a sense from loose to tight intervals. Nc-1, Nc-2, and Nc-3 represent intermediate, loose, and tight intervals, respectively. The capillary number was studied is thought to define a suitable

Table 7. Summary of cumulative oil and water production of the models and core-flood.

	Capillary number set	Cml. oil prod. [cm^3]	Cml. water prod. [cm^3]	Error [%]	
				Oil	Water
Nc-1	−5 −3 −2.5	7.38	152.59	1.07	0.03
Nc-2	−6 −3 −1	8.03	151.95	7.64	0.39
Nc-3	−4.5 −4 −3.5	8.04	151.93	7.77	0.40
Core-flood	−	7.46	152.54	−	−

Fig. 8. Oil production rate and water-cut.

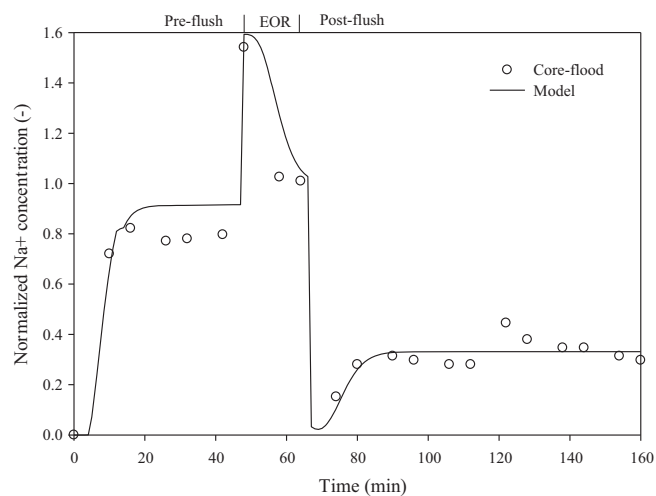**Fig. 9.** Normalized Na concentration.

range that fits in the dynamic production of oil and water. As a result, Nc-1 gave the closest fitting in both cumulative oil and water productions (Fig. 7). Cumulative oil and water productions of Nc-1 are 7.46 and 152.54 cm^3, which thereby give a relative error of 1.07% and 0.03%, respectively.

However, Nc-2 and Nc-3 represented the loose and tight intervals both resulted in an overestimation of cumulative oil and underestimation of cumulative water production. The relative errors of Nc-2 and Nc-3 are 7.64%, 0.39%, and 7.77%, 0.40% for cumulative oil and water production, respectively. In this regard, Nc-1 was selected for further investigation.

4.2 Dynamic history matching of producing effluent

To thoroughly validate the constructed model, producing effluent is required to monitor. The producing effluent includes oil and water producing rate, sodium Na ion tracking, and SDBS concentration at the producing end. Figure 8 depicts the oil production rate and water-cut results.

The dynamic fitting of oil production rate and water-cut revealed a good match. During waterflooding, 1 cm^3/min of oil was initially produced followed by a drastic drop to around 0 after approaching residual oil saturation. Upon injection of SDBS (0.1 wt.%), there was an increase in oil rate around 0.03 cm^3/min. Later after chasing with LSW (1 wt.% NaCl), the oil rate gradually decreased and

produced no more oil later. The observation of water-cut showed the same trend. Moreover, sodium (Na) ion was tracking on a normalized concentration as shown in Figure 9.

It could be seen that tracking of Na ion advancing through the formation shows a good agreement between core-flood and simulation results. A portion of Na adsorbed from an aqueous solution during waterflooding. It then spiked due to the injection of SDBS. It was then released by the injection of SDBS solution due to the high contrast of Na concentration between the displacing and *in-situ* phases. Na ion was then adsorbed within the formation again during LSW injection.

SDBS concentration was equally determined at the production end. Figure 10 illustrates the tracking concentration during production.

Simulation results matched with the core-flood test. The SDBS was injected at 48 min so that the breakthrough time detecting at around 64 min followed by an SDBS bank that reached a peak around 96 min. It was observed that the desorbed SDBS was then drastically decreased and reached 0 ppm around 120 min.

Overall, matching results of producing effluent gave a good agreement between core-flooding and simulation. The relationship between oil rate (and water-cut) and Na and SDBS concentration further validated the constructed model. Therefore, the model was utilized to study the effectiveness of other injection schemes.
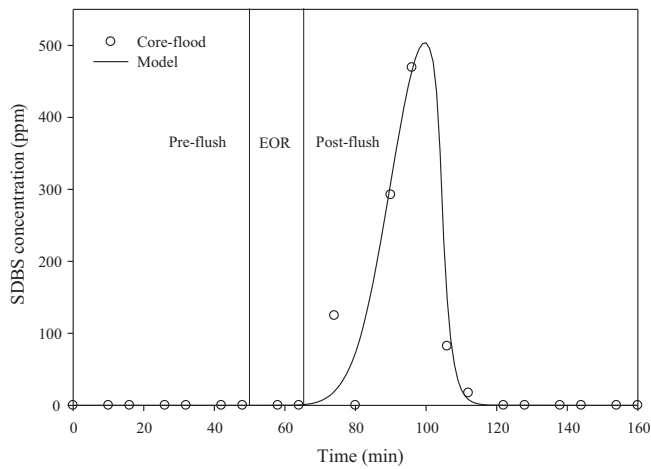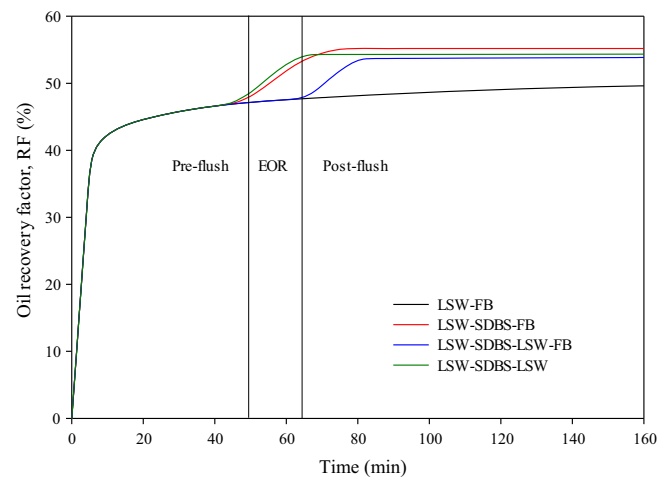
Fig. 10. SDBS concentration.

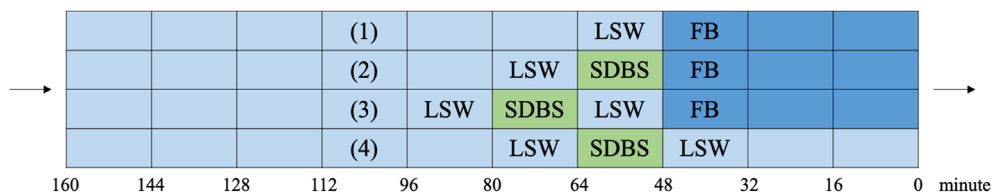**Fig. 12.** RF by various injection schemes.

Fig. 11. Illustration of injection schemes (1) LSW-FB, (2) LSW-SDBS-FB, (3) LSW-SDBS-LSW-FB, (4) LSW-SDBS-LSW.

4.3 Injection schemes

As for a point of validation, the proposed scenario was equally compared with other possible schemes in the reservoir simulation. Figure 11 illustrates the studied injection scheme in comparison to other possible sequences.

The first injection scheme begins with an initial injection of FB followed by an LSW. The LSW was found to increase RF by multi-component ion exchange, wettability alteration, and other mechanisms [42]. The second scheme, the main scenario of this study, includes an SDBS solution prior to LSW injection. The third scheme adds an LSW before the SDBS solution aims at preventing SDBS adsorption that is affected by the degree of salinity. The fourth scheme, FB was replaced by LSW. SDBS is then sandwiching by LSWs. The simulation results showed in Figure 12.

For the first case (LSW-FB), LSW was injected after FB, and the total RF was 49.6%. In the proposed scheme (LSW-SDBS-FB) of our study, SDBS slug was added before LSW, the RF thereby increased 5.6% owing to the IFT reduction.

In comparison to the third scheme (LSW-SDBS-LSW-FB), for instance, LSW was pre-injected after FB to reduce SDBS adsorption. The total RF was 53.8%, which is 1.4% lower than our proposed scheme. The lower RF was due to the lower oil saturation after LSW injection that affects the effectiveness of SDBS flooding. The same observation was also reported by literature [43]. Besides, the oil production was delayed due to the low saline water pre-injection. From the economic point of view, this affects the value of produced oil.

In the last case (LSW-SDBS-LSW), FB was eliminated, which was replaced by LSW since the initial stage, gave an RF of 54.3%. Oil production was observed a small increase upon surfactant injection, yet the total RF was 0.9% lower than which of our proposed scheme (Fig. 12). The key here was owing to the integrated effects of salinity and SDBS desorption. LSW injection modeled the MIE effect found in chemistry analysis (Fig. 4). Desorbed SDBS plays a key role to lower IFT, hence improve RF.

From the simulation results, it is rational to conclude that surfactant desorption is very important to enhance oil production. Increasing surfactant reversibility by introducing the favorable degree saline water, leads to the prolong the low IFT condition within the formation, which is the key to release the trapped oil.

5 Conclusion

This study focuses on the unavoidable problem in surfactant EOR where a portion of injected surfactant is lost to the porous media due to the adsorption onto pore surfaces. We incorporate an approach, LSW-SDBS-FB, where low salinity water injecting after surfactant adsorption. The key findings are summarized as follows:

1. Injecting low salinity water after surfactant adsorption (LSW-SDBS-FB) recovered up to 56.2% of trapped oil, which is 5.3% and 5% greater than high salinity water post-flush (HSW-SDBS-FB) and low salinity water pre-flush (LSW-SDBS-LSW).

2. The proposed scheme was found to develop the second desorbed SDBS slug by Na ion substitution. This reduced IFT of the effluent against the oil sample to 1.3 mN/m.
3. Various injection schemes were studied within the history matched model, LSW-SDBS-FB was confirmed to produce more pronounced RF.

References

1 Deng X., Tariq Z., Murtaza M., Patil S., Mahmoud M., Kamal M.S. (2021) Relative contribution of wettability alteration and interfacial tension reduction in EOR: A critical review, *J. Mol. Liq.* **325**, 115175.

2 Ding F., Gao M. (2021) Pore wettability for enhanced oil recovery, contaminant adsorption and oil/water separation: A review, *Adv. Colloid Interface Sci.* **289**, 102377.

3 Xiong Y., Winterfeld P., Wang C., Huang Z., Wu Y.-S. (2015) Effect of large capillary pressure on fluid flow and transport in stress-sensitive tight oil reservoirs, in: *SPE Annual Technical Conference and Exhibition, 28 September 2015, Houston.*

4 Hu D., Wyatt D., Chen C., Martysevich V. (2015) Correlating recovery efficiency to pore throat characteristics using digital rock analysis, in: *SPE Digital Energy Conference and Exhibition, 3 March 2015, The Woodlands, Texas.*

5 Delshad M., Bhuyan D., Pope G.A., Lake L.W. (1986) Effect of capillary number on the residual saturation of a three-phase micellar solution, in: *SPE Enhanced Oil Recovery Symposium, 20 April 1986, Tulsa, Oklahoma.*

6 Yuan C.-D., Pu W.-F., Wang X.-C., Sun L., Zhang Y.-C., Cheng S. (2015) Effects of interfacial tension, emulsification, and surfactant concentration on oil recovery in surfactant flooding process for high temperature and high salinity reservoirs, *Energy Fuel* **29**, 10, 6165–6176.

7 Jang J., Sun Z., Santamarina J.C. (2016) Capillary pressure across a pore throat in the presence of surfactants, *Water Resour. Res.* **52**, 12, 9586–9599.

8 Nguele R., Sasaki K., Sugai Y., Omondi B., Said Al-Salim H., Ueda R. (2016) Interactions between formation rock and petroleum fluids during microemulsion flooding and alteration of heavy oil recovery performance, *Energy Fuel* **31**, 1, 255–270.

9 Mohamed A.I.A., Sultan A.S., Hussein I.A., Al-Muntasheri G.A. (2017) Influence of Surfactant Structure on the Stability of Water-in-Oil Emulsions under High-Temperature High-Salinity Conditions, *J. Chem.* **2017**, 5471376.

10 Mandal A., Samanta A., Bera A., Ojha K. (2010) Role of oil-water emulsion in enhanced oil recovery, in: *2010 International Conference on Chemistry and Chemical Engineering*, pp. 190–194.

11 Zhao H., Yang H., Kang X., Jiang H., Li M., Kang W., Sarsenbekuly B. (2020) Study on the types and formation mechanisms of residual oil after two surfactant imbibition, *J. Pet. Sci. Eng.* **195**, 107904.

12 Karnanda W., Benzagouta M.S., AlQuraishi A., Amro M.M. (2013) Effect of temperature, pressure, salinity, and surfactant concentration on IFT for surfactant flooding optimization, *Arab. J. Geosci.* **6**, 9, 3535–3544.

13 Kalam S., Abu-Khamsin S.A., Kamal M.S., Patil S. (2021) A review on surfactant retention on rocks: mechanisms, measurements, and influencing factors, *Fuel* **293**, 120459.

14 Ngo I., Sasaki K., Nguele R., Sugai Y. (2019) Improving surfactant EOR by water salinity alteration, *ASEG Ext. Abstr.* **2019**, 1, 1–4.

15 Paternina C.A., Londoño A.K., Rondon M., Mercado R., Botett J. (2020) Influence of salinity and hardness on the static adsorption of an extended surfactant for an oil recovery purpose, *J. Pet. Sci. Eng.* **195**, 107592.

16 Ngo I., Srisuriyachai F., Sugai Y., Sasaki K. (2017) Study of heterogeneous reservoir effects on surfactant flooding in consideration of surfactant adsorption reversibility, in: *SPWLA 23rd Formation Evaluation Symposium of Japan, Chiba, Japan, 11–12 October 2017.*

17 Ngo I., Srisuriyachai F., Sasaki K., Sugai Y., Nguele R. (2019) Effects of Reversibility on Enhanced Oil Recovery Using Sodium Dodecylbenzene Sulfonate (SDBS), *J. Japan Pet. Inst.* **62**, 4, 188–198.

18 Islam M.S., Kleppe J., Rahman M.M., Abbasi F. (2018) An evaluation of IOR potential for the Norne Field's E-segment using low salinity water-flooding: A case study, in: *SPE Kingdom of Saudi Arabia Annual Technical Symposium and Exhibition.*

19 Pollen E.N., Berg C.F. (2018) Experimental investigation of osmosis as a mechanism for low-salinity EOR, in: *Abu Dhabi International Petroleum Exhibition & Conference, 2018.*

20 Ain Binti Mohd Anuar N., Hussinyunan M., Sagala F., Katende A. (2017) The effect of WAG ratio and oil density on oil recovery by immiscible water alternating gas flooding citation the effect of WAG ratio and oil density on oil recovery by immiscible water alternating gas flooding, *Am. J. Sci. Technol.* **4**, 5, 80–90.

21 Alagic E., Skauge A. (2010) Combined low salinity brine injection and surfactant flooding in mixed-wet sandstone cores, *Energy Fuel* **24**, 6, 3551–3559.

22 Sheng J.J. (2014) Critical review of low-salinity waterflooding, *J. Pet. Sci. Eng.* **120**, 216–224.

23 Fattahi Mehraban M., Ayatollahi S., Sharifi M. (2019) Role of divalent ions, temperature, and crude oil during water injection into dolomitic carbonate oil reservoirs, *Oil Gas Sci. Technol. – Rev. IFP Energies nouvelles* **74**, 36.

24 Zaheri S.H., Khalili H., Sharifi M. (2020) Experimental investigation of water composition and salinity effect on the oil recovery in carbonate reservoirs, *Oil Gas Sci. Technol. – Rev. IFP Energies nouvelles* **75**, 21.

25 Egbe D.I.O., Jahanbani Ghahfarokhi A., Nait Amar M., Torsæter O. (2021) Application of low-salinity waterflooding in carbonate cores: a geochemical modeling study, *Nat. Resour. Res.* **30**, 1, 519–542.

26 Song J., *et al.* (2020) Effect of salinity, Mg^{2+} and SO_4^{2-} on "smart water"-induced carbonate wettability alteration in a model oil system, *J. Colloid Interface Sci.* **563**, 145–155.

27 Hosseinzade Khanamiri H., Baltzersen Enge I., Nourani M., Stensen J.Å., Torsæter O., Hadia N. (2016) EOR by low salinity water and surfactant at low concentration: impact of injection and in situ brine composition, *Energy Fuel* **30**, 4, 2705–2713.

28 Tavassoli S., Korrani A.K., Pope G.A., Sepehrnoori K. (2016) Low-salinity surfactant flooding – A multimechanistic enhanced-oil-recovery method, *SPE J.* **21**, 03, 744–760.

29 Araz A., Kamyabi F. (2021) Experimental study of combined low salinity and surfactant flooding effect on oil recovery, *Oil Gas Sci. Technol. – Rev. IFP Energies nouvelles* **76**, 4.

30 Geffroy C., Cohen Stuart M.A., Wong K., Cabane B., Bergeron V. (2000) Adsorption of nonionic surfactants onto polystyrene: Kinetics and reversibility, *Langmuir* **16**, 16, 6422–6430.

31 Somasundaran P., Hanna H.S. (1985) Adsorption/desorption of sulfonate by reservoir rock minerals in solutions of varying sulfonate concentrations, *Soc. Pet. Eng. J.* **25**, 03, 343–350.

32 Chang Z., Chen X., Peng Y. (2018) The adsorption behavior of surfactants on mineral surfaces in the presence of electrolytes – A critical review, *Miner. Eng.* **121**, 66–76.

33 Ansah E.O., Nguele R., Sugai Y., Sasaki K. (2019) Predicting the antagonistic effect between albite-anorthite synergy and anhydrite on chemical enhanced oil recovery: effect of inorganic ions and scaling, *J. Dispers. Sci. Technol.* **42**, 1, 21–32.

34 Kim Y., Kim C., Kim J., Kim Y., Lee J. (2020) Experimental investigation on the complex chemical reactions between clay minerals and brine in low salinity water-flooding, *J. Ind. Eng. Chem.* **89**, 316–333.

35 Bourbiaux B. (2020) Low salinity effects on oil recovery performance: underlying physical mechanisms and practical assessment, *Oil Gas Sci. Technol. – Rev. IFP Energies nouvelles* **75**, 37.

36 Tichelkamp T., Teigen E., Nourani M., Øye G. (2015) Systematic study of the effect of electrolyte composition on interfacial tensions between surfactant solutions and crude oils, *Chem. Eng. Sci.* **132**, 244–249.

37 Chai R., Liu Y., He Y., Cai M., Zhang J., Liu F., Xue L. (2021) Effects and mechanisms of acidic crude oil-aqueous solution interaction in low-salinity waterflooding, *Energy Fuel* **35**, 12, 9860–9872.

38 Ngo I., Nguele R., Sugai Y., Sasaki K. (2021) Investigation on surfactant desorption isotherm to enhance oil spontaneous recovery in a low permeability core, *Int. J. Oil Gas Coal Technol.* **28**, 4, 421–441.

39 Wu Y., Cheng L., Ma L., Huang S., Fang S., Killough J., Jia P., Wang S. (2021) A transient two-phase flow model for production prediction to tight gas wells with fracturing fluid-induced formation damage, *J. Pet. Sci. Eng.* **199**, 108351.

40 Austad T., RezaeiDoust A., Puntervold T. (2010) Chemical mechanism of low salinity water flooding in sandstone reservoirs, in: *SPE Improved Oil Recovery Symposium, 24 April 2010, Tulsa, Oklahoma.*

41 Sheng J.J. (2011) *Modern chemical enhanced oil recovery: theory and practice*, Elsevier, Burlington.

42 Katende A., Sagala F. (2019) A critical review of low salinity water flooding: Mechanism, laboratory and field application, *J. Mol. Liq.* **278**, 627–649.

43 Druetta P., Picchioni F. (2019) Surfactant flooding: The influence of the physical properties on the recovery efficiency, *Petroleum* **6**, 149–162.